ELSEVIER

International Journal of Cardiology 109 (2006) 430 – 431

International Journal of Cardiology

www.elsevier.com/locate/ijcard

Letter to the Editor

Endocardial fibrosis in subacute non-Q wave myocardial infarction demonstrated by multislice computed tomography

Nobusada Funabashi*, Nobuyuki Komiyama, Miki Asano, Issei Komuro

Department of Cardiovascular Science and Medicine, Chiba University Graduate School of Medicine, 1-8-1 Inohana, Chuo-ku, Chiba City, Chiba 260-8670, Japan

Received 24 March 2005; accepted 1 April 2005
Available online 10 May 2005

Keywords: Endocardial fibrosis; Subacute non Q-wave myocardial infarction; Multislice computed tomography

Several diagnostic modalities such as echocardiography [1], magnetic resonance imaging (MRI) [2], single photon emission computed tomography (SPECT) [3], and positron emission tomography (PET) [4], can be used to evaluate infarcted myocardium. However, it is difficult to accurately distinguish the location of the infarct in the myocardium, such as in non-Q wave myocardial infarction (MI), which suggests an endocardial MI rather than a transmural MI.

A 57-year-old man had an anteroseptal MI 15 years ago. Recently, he had a second MI with new ST segment depressions and inverted T waves on ECG in the lateral precardial leads. Conventional coronary angiograms revealed complete occlusion of the proximal portion of the LAD and the collateral branches to the peripheral arteries of the LAD from the left circumflex branch (Fig. 1). The proximal portion of the obtuse marginal (OM) branch was totally occluded. The peripheral portion of the OM was observed by blood flow from the collateral arteries from the posterior lateral branch. We were unable to determine which arteries were responsible for the infarction from the angiographic data.

To clarify the location of the non-Q wave infarct site, enhanced ECG gated multislice computed tomography (CT) (Aquilion, Toshiba) was performed with a 1-mm slice thickness and a helical pitch of 1.0. Routine scanning was performed with intravenous injection of 100ml of iodinated contrast material (300 mg I/ml), at 30 s and 7 min after the injection. The CT revealed late enhancement of the endocardial portion of the lateral apex of the left ventricle, which were hypodense in the early phase (arrows, Fig. 2). This region still exhibited normal myocardial thickness at the epicardial site. This indicated that reconstruction of the interstitium, possibly fibrotic changes, had occurred in this region. Endocardial fibrotic changes observed by CT with the findings of the

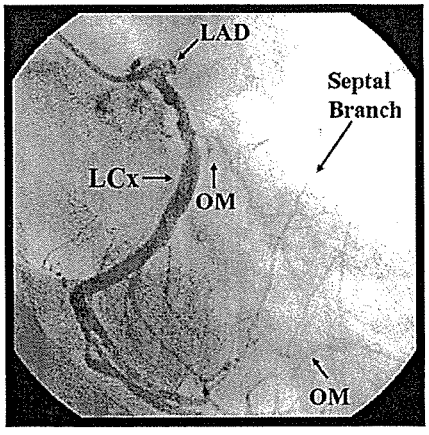

Fig. 1. Conventional coronary angiogram revealed an occlusion of the proximal portion of the left anterior descending branch (LAD) and the collateral branches to the peripheral arteries of the LAD through the septal branches from the left posterior descending branch. The proximal portion of the obtuse marginal branch (OM) was totally occluded (arrowhead) and the peripheral branch of OM was observed by the collateral flow from the posterior lateral branch. LCx, left circumflex branch.

* Corresponding author.
E-mail address: nobusada@ma.kcom.ne.jp (N. Funabashi).

0167-5273/$ - see front matter
doi:10.1016/j.ijcard.2005.04.013

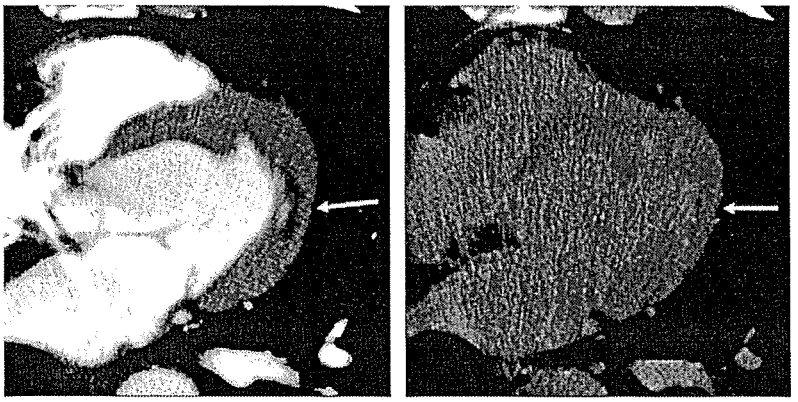

Fig. 2. Axial source images of electrocardiogram-gated multislice computed tomography (CT) from end-diastole in the early (A) and late (B) phases after injection of the contrast material. The endocardial portion of the lateral apex of the left ventricle revealed hypodense CT values during the early phase after the injection of the contrast material (arrows). Normal myocardial thickness at the epicardial site was still evident and enhancement occurred only in the late phase. This area consisted of interstitial changes such as fibrosis or edema and appeared not to be transmural, since this region still exhibited normal myocardial thickness at the epicardial site with isodense CT values that were the same as seen on images of other normal myocardia.

ECG and coronary angiograms suggested that the culprit coronary artery in this event must be the OM.

Detection of the location of an endocardial infarct in the myocardium is difficult, as non Q wave MI frequently occurs in subjects with multi-vessel disease of the coronary arteries, and thus, it may be difficult to distinguish the responsible vessels causing non Q wave MI. Therefore, it is very important to clearly distinguish the location of the infarct area as transmural or localized in the endocardium. Such diagnosis may help to prepare a strategy for percutaneous transmural coronary intervention.

ECG-gated multislice CT has a better spatial resolution than MRI, SPECT, and PET [5], and using characteristics of iodinated contrast material, which shows defect in the early phase and abnormal enhancement in the late phase in myocardial fibrosis [6], it is possible to detect the location of the endocardial fibrosis, which helps to determine which arteries are responsible for the infarction.

References

[1] Park SW, Lee SY, Park SJ, Lee SC, Gwon HC, Kim DK. Quantitative assessment of infarct size in vivo by myocardial contrast echocardiography in a murine acute myocardial infarction model. Int J Cardiol 2004;97(3):393–8.

[2] Ogawa E, Okinaka T, Motoyasu M, et al. A case of acute myocardial infarction caused by left main trunk disease with dilated cardiomyopathy. Int J Cardiol 2005;98(3):507–8.

[3] Fiorina P, Pattoneri P, Paganelli C, Secchi A, Calbiani B, Astorri E. Correlation between non-reversible thallium-201 myocardial perfusion defect and ECG criteria in the diagnosis of apical myocardial infarction. Int J Cardiol 2004;95(2–3):251–4.

[4] Yoshida K, Gould KL. Quantitative relation of myocardial infarct size and myocardial viability by positron emission tomography to left ventricular ejection fraction and 3-year mortality with and without revascularization. J Am Coll Cardiol 1993;22(4):984–97.

[5] Ratti C, Barbieri A, Ligabue G, et al. Non-invasive, three-dimensional visualization of coronary artery bypass grafts by multislice spiral computed tomography. Int J Cardiol 2005;99(1):157–9.

[6] Masuda Y, Yoshida H, Morooka N, Watanabe S, Inagaki Y. The usefulness of X-ray computed tomography for the diagnosis of myocardial infarction. Circulation 1984;70(2):217–25.

Location of Focal Vasospasm Provoked by Ergonovine Maleate Within Coronary Arteries in Patients With Vasospastic Angina Pectoris

Tomomi Koizumi, MD, PhD[a], Masaki Yokoyama, MD, PhD[b], Susumu Namikawa, MD, PhD[b], Nehiro Kuriyama, MD, PhD[b], Mizuo Nameki, MD, PhD[b], Takashi Nakayama, MD[b], Hideaki Kaneda, MD, PhD[a], Krishnankutty Sudhir, MD, PhD[a], Paul G. Yock, MD[a], Nobuyuki Komiyama, MD, PhD[c], and Peter J. Fitzgerald, MD, PhD[a,*]

This study examined whether coronary focal vasospasm occurs in a nonuniform distribution within the coronary tree and whether a longitudinal plaque distribution pattern is present in patients with vasospastic angina using 3-dimensional intravascular ultrasound analysis. Of 121 patients with clinically suspected angina without fixed stenosis in the coronary arteries, vasospasm was provoked in 82 patients with 92 lesions (42 focal, 50 diffuse) by intravenous ergonovine maleate injection. Most focal vasospasms occurred in the proximal third of the coronary arteries (proximal 28, mid 8, distal 6, $p < 0.01$), corresponding to the historical high-risk zones for acute coronary occlusion. More plaque burden also existed in the proximal third of the coronary arteries in patients with focal vasospasm. (Am J Cardiol 2006;97:1322–1325)

Vasospasm in coronary arteries has been shown to play an important role in the pathogenesis of not only variant angina, but also acute myocardial infarction, fatal arrhythmia, and sudden cardiac death.[1–3] Focal vasospasm has been associated with a significantly higher incidence of cardiac events than diffuse vasospasm.[4] A recent report has shown that acute coronary occlusions tend to cluster in a predictable high-risk zone within the proximal third of the coronary arteries.[5] However, the geographic evaluation of the site of focal vasospasm in the coronary artery has not been fully elucidated. Moreover, the longitudinal plaque distribution pattern has not been examined in patients with vasospastic angina using 3-dimensional intravascular ultrasound (IVUS) analysis.

• • •

Provocation of vasospasm by intravenous ergonovine maleate administration was performed in 121 patients with clinically suspected angina, without fixed stenosis in the coronary arteries, after admission to the Center for Cardiovascular Interventions, Chiba University Hospital, Chiba, Japan. After the patients provided informed consent, cardiac catheterization, coronary angiography, and a subsequent coronary vasospasm provocation test were performed as a part of the diagnostic procedure. All medications, except for emergency sublingual nitroglycerin, were discontinued ≥24 hours before cardiac catheterization. After administration of diazepam 5 mg for sedation, patients were taken to the catheterization laboratory. Any drugs likely to affect coronary hemodynamics were not used during the catheterization procedure before selective coronary angiography. Standard cardiac catheterization, including pressure recording, left ventriculography, and selective coronary angiography, was performed after intravenous injection of 2,000 to 3,000 U of heparin.

After confirmation of no luminal narrowing of >50% in the coronary artery by control coronary angiography, 0.2 mg of ergonovine maleate was administrated intravenously to provoke vasospasm. A standard 12-lead electrocardiogram was used for monitoring during coronary angiography to detect any ST-T segment changes. Immediately after chest pain with ST-T segment elevation or ST depression of >0.1 mV was observed or 3 minutes after ergonovine maleate was injected, coronary angiography was performed to confirm the provocation of vasospasm. Subsequently, 100 to 200 μg of intracoronary nitroglycerin was injected to relieve the vasospasm. Coronary angiography and intracoronary injection of nitroglycerin were repeated until the coronary vasospasm was completely relieved.

Of the 92 lesions in 82 patients with positive results, 42 had focal vasospasm, defined as a discrete transient narrowing of >90% that was localized to coronary arteries and associated with ST-T segment elevation or depression of >0.1 mV by 12-lead electrocardiography. The remaining 50 lesions were classified as nonfocal (i.e., diffuse vasoconstriction or diffuse vasospasm) that was diagnosed when a transient vessel narrowing of >90% compared with the control coronary angiogram was observed from the proximal to distal segment in the 3 major coronary arteries, with

[a]Center for Research in Cardiovascular Interventions, Division of Cardiovascular Medicine, Stanford University, Stanford, California; [b]Center for Cardiovascular Interventions, Chiba University Hospital, Chiba; and [c]Division of Cardiology, Saitama Medical School, Saitama, Japan. Manuscript received August 31, 2005; revised manuscript received and accepted November 15, 2005.

* Corresponding author: Tel: 650-498-6034; fax: 650-498-6027.
E-mail address: ivus@crci.stanford.edu (P.J. Fitzgerald).

0002-9149/06/$ – see front matter
doi:10.1016/j.amjcard.2005.11.073

Table 1
Clinical characteristics

Variable	Spasm Type		p Value
	Diffuse (n = 47)	Focal (n = 35)	
Age (yrs)	58.6 ± 6.2	56.3 ± 9.8	0.19
Men	26 (55%)	29 (83%)	<0.01
Smoker	21 (45%)	18 (51%)	0.55
Diabetes mellitus	5 (11%)	3 (9%)	0.76
Hypertension*	7 (15%)	3 (9%)	0.38
Hypercholesterolemia†	19 (40%)	5 (14%)	0.01

Data are presented as mean ± SD or numbers (percentages).

* Defined as use of antihypertensive therapy or systolic blood pressure >140 mm Hg.

† Defined as fasting total cholesterol level >220 mg/dl or use of lipid-lowering therapy.

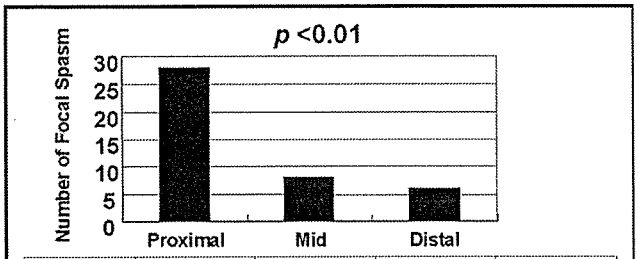

LAD	13	6	0	p=0.01
LCX	11	0	3	p=0.06
RCA	4	2	3	p=0.84

Figure 1. Site distribution of focal vasospasm in epicardial coronary tree. Overall, focal vasospasm clustered within the proximal third of the coronary artery (proximal 28, mid 8, distal 6, p <0.01). Sites of focal vasospasm in the left anterior descending artery (LAD; proximal 13, mid 6, distal 0, p = 0.01) and left circumflex artery (LCX; proximal 11, mid 0, distal 3, p = 0.06) were nonuniform. In contrast, sites of focal vasospasm in the right coronary artery (RCA) were uniform (proximal 4, mid 2, distal 3, p = 0.84).

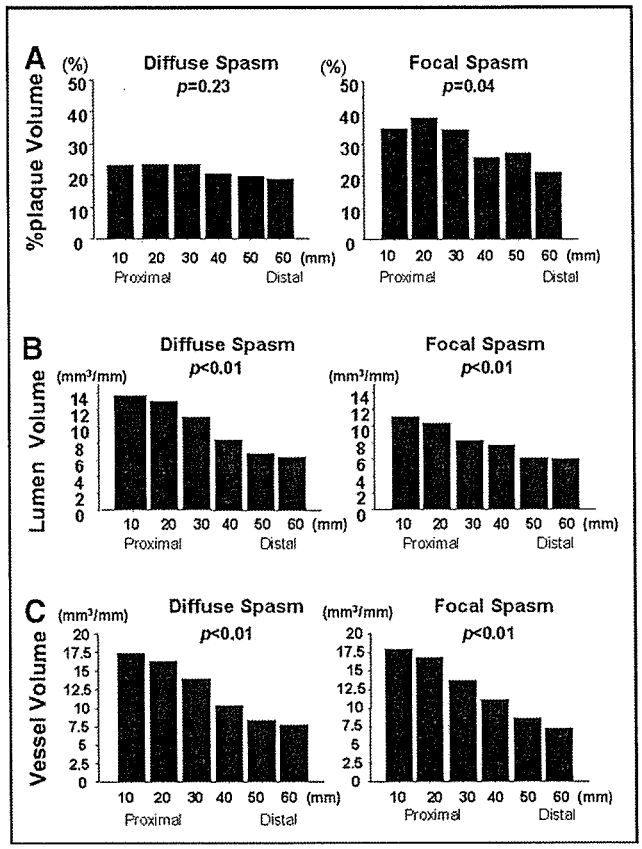

Figure 2. *(A)* Distribution of percentage of plaque volume in each 10-mm section from ostium to 60 mm distally of coronary artery. *Left*, diffuse vasospasm. Uniform distribution of percentage of plaque volume (p = 0.23). *Right*, focal vasospasm. Nonuniform distribution of percentage of plaque volume (p = 0.04) predominantly in proximal 30 mm. *(B, C)* Distribution of lumen volume and vessel volume in each 10-mm section from ostium to 60 mm distally of coronary artery. In diffuse and focal vasospasm, lumen volume and vessel volume tapered significantly from the ostium to 60 mm distally (p <0.01).

or without discrete changes in the coronary diameter in the small branches, in association with ST elevation or depression of >0.1 mV by 12-lead electrocardiography. Transient vasoconstriction of >25% compared with the control angiogram after administration of ergonovine maleate was considered a negative test finding.

The site of focal vasospasm in each epicardial coronary artery was classified into 3 locations (proximal, mid, or distal) according to the coronary artery map from the American Heart Association classification.[6]

In a subset of 26 patients, IVUS was performed to examine the longitudinal plaque distribution pattern in patients with vasospastic angina, using a 2.9-Fr, 40-MHz, single-element, mechanical ultrasound catheter (Boston Scientific, Natick, Massachusetts) with motorized pull-back devices (0.5 mm/s). Per protocol, intracoronary nitroglycerin was injected before image acquisition. Twenty-two IVUS images could be recorded from the coronary artery ostium to a distance of >60 mm distally on s-VHS videotape for off-line analysis. Three-dimensional reconstruction of the IVUS images was performed using a commercially available quantitative analysis system, which runs on an Intel Pentium-based personal computer system with Windows NT (echoPlaque, version 2.9, INDEC Systems, Mountain View, California). After digitization of the IVUS recordings at a frame rate of 15 images/s, longitudinal views of the studied segments were automatically processed by the system. The lumen and external elastic membrane areas were manually delineated from the ostium to a distance of >60 mm distally at 16-frame intervals, and the interpolated measurements of the remaining frames were automatically generated. Using Simpson's method, the lumen volume and vessel volume inside the external elastic membrane were calculated. The percentage of plaque volume of each 10 mm from the ostium to 60 mm distally of the coronary artery was obtained with the following formula: ([vessel volume − lumen volume]/vessel volume) × 100.

The means ± SDs are presented for continuous data. The chi-square test was used to compare the categorical vari-

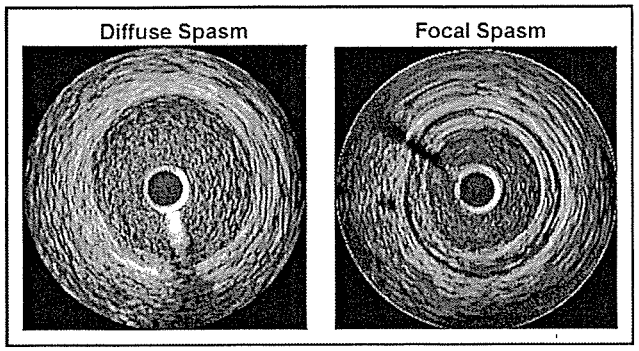

Figure 3. *Left*, Cross-sectional IVUS image at site of diffuse vasospasm in proximal left anterior descending coronary artery showing no intima-media thickening (i.e., normal appearance). *Right*, cross-sectional image of site of focal vasospasm in proximal left anterior descending coronary artery showing concentric intima-media thickening with qualitatively fibrofatty tissue.

ables. Analysis of variance was used to test whether the locations of focal vasospasm and plaque burden were uniformly distributed in the coronary arteries. A p value of <0.05 was considered statistically significant.

The demographic data are reported in Table 1. In this study, the prevalence of coronary risk factors was comparable between the patients with focal and diffuse vasospasms, except that the group with focal vasospasm had more men ($p < 0.01$) and less frequent hypercholesterolemia ($p = 0.01$), defined as a fasting total cholesterol level of >220 mg/dl or the use of lipid-lowering therapy.

Overall, the site of focal vasospasm was clustered within the proximal third of the coronary arteries ($p < 0.01$; Figure 1). The site of focal vasospasm in the left anterior descending artery ($p = 0.01$) and left circumflex artery ($p = 0.06$) was nonuniform, despite uniform distribution in the right coronary artery ($p = 0.84$). Plaque was distributed nonuniformly in the proximal third of the coronary arteries in patients with focal vasospasm ($n = 10$, $p = 0.04$), although plaque was distributed uniformly in patients with diffuse vasospasm ($n = 12$, $p = 0.23$). The lumen and vessel area tapered similarly in the 2 groups (Figure 2). Cross-sectional IVUS images at the site of vasospasm in the proximal left anterior descending artery are shown in Figure 3.

• • •

Schroeder et al[7] first described focal and nonfocal coronary arterial spasm during administration of ergonovine maleate in 1977. They had already recognized that these 2 patterns of vasospasm typically have a different appearance on angiography.[7] After that, some investigators demonstrated the pathophysiology of coronary spasm, especially of focal vasospasm. Heupler[8] suggested that even in the absence of angiographic disease, occult atherosclerotic lesions could be present at the sites of focal coronary spasm. This finding was proved by IVUS studies showing minimal atherosclerotic lesions at the site of focal spasm.[9] Coronary focal spasm is caused by local hyperreactivity to a generalized constrictor stimulus on minimal atherosclerosis.[10] Also, at the site of focal vasospasm, erosion, ulcer, or thrombus was detected by coronary angioscopy in locally injured coronary arteries.[11] From a prognostic viewpoint of vasospastic angina, focal vasospasm has been associated with a significantly higher incidence of cardiac events, including sudden death, myocardial infarction, and unstable angina, than diffuse vasospasm.[4]

Under these clinical conditions, previous studies have suggested that focal vasospasm might be associated with more advanced atherosclerosis than diffuse vasospasm in patients with vasospastic angina. Thus, providing a complete longitudinal view of plaque inside the vessel to better evaluate the site of focal vasospasm within the coronary artery would benefit our understanding of this clinical situation.

A recent report has shown that acute coronary thrombotic occlusions (due to plaque rupture) leading to ST-elevation myocardial infarction are clustered within the proximal third of the coronary arteries.[5] Also, most vulnerable plaques occur predominantly in the proximal portion of the 3 major coronary arteries.[12] Furthermore, Hong et al,[13] using IVUS, found that plaque ruptures occurred mainly in the proximal segments of the left anterior descending artery (83% of the plaque ruptures were 10 to 40 mm from the ostium) and the proximal and distal segments of the right coronary artery (48% of the plaque ruptures were 10 to 40 mm from the ostium and 32% of the plaque ruptures were >70 mm from the ostium). These data are similar to our results that focal spasm occurred mainly in the proximal (68%) segment of the left anterior descending artery and the proximal (44%) and distal (33%) segments of the right coronary artery. Considering that plaque ruptures represent only 2/3 of the causes of coronary thrombosis,[14,15] focal coronary spasm and plaque rupture may play an important role in the pathogenesis of acute myocardial infarction, respectively, or simultaneously. Additional research is needed to examine the contribution of focal vasospasm to plaque rupture at these sites.

We have also shown that an increased plaque burden exists in the proximal third of the coronary arteries in patients with focal vasospasm using 3-dimensional IVUS analysis. This plaque accumulation might progress and represent a vulnerability to plaque rupture, leading to acute coronary occlusion.[16] Because the lumen areas tapered similarly in the 2 groups, angiography could not reveal the plaque accumulation in the proximal segments of the coronary arteries. Taking into account the results that acute myocardial infarctions occur frequently in angiographically normal-looking segments,[17] IVUS may be a useful tool for detecting plaque severity.

Acknowledgment: We thank Heidi N. Bonneau, RN, MS, for her expert review of the manuscript.

1. Myerburg RJ, Kessler KM, Mallon SM, Cox MM, deMarchena E, Interian A Jr, Castellanos A. Life-threatening ventricular arrhythmias in patients with silent myocardial ischemia due to coronary-artery spasm. *N Engl J Med* 1992;326:1451–1455.
2. Roberts WC, Curry RC Jr, Isner JM, Waller BF, McManus BM, Mariani-Constantini R, Ross AM. Sudden death in Prinzmetal's angina with coronary spasm documented by angiography: analysis of three necropsy patients. *Am J Cardiol* 1982;50:203–210.
3. Suzuki H, Kawai S, Aizawa T, Kato K, Sunayama S, Okada R, Yamaguchi H. Histological evaluation of coronary plaque in patients with variant angina: relationship between vasospasm and neointimal hyperplasia in primary coronary lesions. *J Am Coll Cardiol* 1999;33: 198–205.
4. Mori F, Uchida T, Byun T, Tanino S, Imamura K, Oomori H, Nagashima M, Enta K, Tanaka M, Kasahara S, Hirosawa K. Cardiac events in vasospastic angina: site and morphology of coronary artery spasm is related to the long-term prognosis of vasospastic angina. *J Cardiol* 1999;33:191–199.
5. Wang JC, Normand SL, Mauri L, Kuntz RE. Coronary artery spatial distribution of acute myocardial infarction occlusions. *Circulation* 2004;110:278–284.
6. Austen WG, Edwards JE, Frye RL, Gensini GG, Gott VL, Griffith LS, McGoon DC, Murphy ML, Roe BB. A reporting system on patients evaluated for coronary artery disease: report of the Ad Hoc Committee for Grading of Coronary Artery Disease, Council on Cardiovascular Surgery, American Heart Association. *Circulation* 1975;51:5–40.
7. Schroeder JS, Bolen JL, Quint RA, Clark DA, Hayden WG, Higgins CB, Wexler L. Provocation of coronary spasm with ergonovine maleate: new test with results in 57 patients undergoing coronary arteriography. *Am J Cardiol* 1977;40:487–491.
8. Heupler FA Jr. Syndrome of symptomatic coronary arterial spasm with nearly normal coronary arteriograms. *Am J Cardiol* 1980;45:873–881.
9. Yamagishi M, Miyatake K, Tamai J, Nakatani S, Koyama J, Nissen SE. Intravascular ultrasound detection of atherosclerosis at the site of focal vasospasm in angiographically normal or minimally narrowed coronary segments. *J Am Coll Cardiol* 1994;23:352–357.
10. Kaski JC, Maseri A, Vejar M, Crea F, Hackett D. Spontaneous coronary artery spasm in variant angina is caused by a local hyperreactivity to a generalized constrictor stimulus. *J Am Coll Cardiol* 1989;14: 1456–1463.
11. Etsuda H, Mizuno K, Arakawa K, Satomura K, Shibuya T, Isojima K. Angioscopy in variant angina: coronary artery spasm and intimal injury. *Lancet* 1993;342:1322–1324.
12. Narula J, Finn AV, Demaria AN. Picking plaques that pop. *J Am Coll Cardiol* 2005;45:1970–1973.
13. Hong MK, Mintz GS, Lee CW, Lee BK, Yang TH, Kim YH, Song JM, Han KH, Kang DH, Cheong SS, et al. The site of plaque rupture in native coronary arteries: a three-vessel intravascular ultrasound analysis. *J Am Coll Cardiol* 2005;46:261–265.
14. Farb A, Burke AP, Tang AL, Liang TY, Mannan P, Smialek J, Virmani R. Coronary plaque erosion without rupture into a lipid core: a frequent cause of coronary thrombosis in sudden coronary death. *Circulation* 1996;93:1354–1363.
15. Burke AP, Farb A, Malcom GT, Liang YH, Smialek J, Virmani R. Coronary risk factors and plaque morphology in men with coronary disease who died suddenly. *N Engl J Med* 1997;336:1276–1282.
16. Nobuyoshi M, Tanaka M, Nosaka H, Kimura T, Yokoi H, Hamasaki N, Kim K, Shindo T, Kimura K. Progression of coronary atherosclerosis: is coronary spasm related to progression? *J Am Coll Cardiol* 1991;18:904–910.
17. Nissen SE, Yock P. Intravascular ultrasound: novel pathophysiological insights and current clinical applications. *Circulation* 2001;103:604–616.

Int J Cardiovasc Imaging
DOI 10.1007/s10554-007-9212-1

ORIGINAL PAPER

Quantitative colorimetry of atherosclerotic plaque using the L*a*b* color space during angioscopy for the detection of lipid cores underneath thin fibrous caps

Fumiyuki Ishibashi · Shinya Yokoyama · Kengo Miyahara · Alexandra Dabreo · Eric R. Weiss · Mark Iafrati · Masamichi Takano · Kentaro Okamatsu · Kyoichi Mizuno · Sergio Waxman

Received: 24 November 2006 / Accepted: 31 January 2007

Abstract
Objectives Yellow plaques seen during angioscopy are thought to represent lipid cores underneath thin fibrous caps (LCTCs) and may be indicative of vulnerable sites. However, plaque color assessment during angioscopy has been criticized because of its qualitative nature. The purpose of the present study was to test the ability of a quantitative colorimetric system to measure yellow color intensity of atherosclerotic plaques during angioscopy and to characterize the color of LCTCs.
Methods Using angioscopy and a quantitative colorimetry system based on the L*a*b* color space [L* describes brightness (–100 to +100), b* describes blue to yellow (–100 to +100)], the optimal conditions for measuring plaque color were determined in three flat standard color samples and five artificial plaque models in cylinder porcine carotid arteries. In 88 human tissue samples, the colorimetric characteristics of LCTCs were then evaluated.
Results In in-vitro samples and ex-vivo plaque models, brightness L* between 40 and 80 was determined to be optimal for acquiring b* values, and the variables unique to angioscopy in color perception did not impact b* values after adjusting for brightness L* by manipulating light or distance. In ex-vivo human tissue samples, b* value ≥23 (35.91 ± 8.13) with L* between 40 and 80 was associated with LCTCs (fibrous caps <100 μm).
Conclusions Atherosclerotic plaque color can be consistently measured during angioscopy with quantitative colorimetry. High yellow color intensity, determined by this system, was associated with LCTCs. Quantitative colorimetry during angioscopy may be used for detection of LCTCs, which may be markers of vulnerability.

Keywords Angioscopy · Quantitative colorimetry · Atherosclerotic plaque · Imaging

F. Ishibashi · A. Dabreo · E. R. Weiss · S. Waxman
Center for Translational Cardiovascular Research, Tufts New England Medical Center, Boston, MA, USA

S. Yokoyama · M. Takano · K. Okamatsu · K. Mizuno
Department of Internal Medicine, Chiba-Hokusoh Hospital, Nippon Medical School, Chiba, Japan

K. Miyahara
Institute of Archaeological Research Kyoto, Kyoto, Japan

M. Iafrati
Department of Vascular Surgery, Tufts New England Medical Center, Boston, MA, USA

S. Waxman (✉)
Lahey Clinic Medical Center, 41 Mall Road, Burlington, MA 01805, USA
e-mail: sergio.waxman@lahey.org

Abbreviations

ACS	Acute coronary syndromes
A/D	Analog to digital
CCD	Charge-coupled device
CIE	International Committee on Illumination
HIS	Hue, saturation, intensity
LCTC	Lipid core underneath thin fibrous cap
NTSC	National Television System Committee
POI	Point of interest
RGB	Red, green, blue
ROI	Region of interest
SD	Standard deviation

Introduction

Lipid cores underneath thin fibrous caps (LCTCs) are found in most ruptured plaques and a majority of culprit lesions of acute coronary syndromes (ACS) [1], and are thought to be the regions which may be vulnerable to thrombosis. Early detection of such regions may potentially lead to prediction and prevention of ACS [2]. LCTCs may appear yellow by angioscopy, based on the association of yellow plaque color with lipid-rich atheromas [3] or thin fibrous caps covering lipid cores [4], as well as clinical studies demonstrating the association of yellow lesions and ACS and thrombus [5–7]. However, use of yellow plaque color by angioscopy as a marker of LCTCs has been limited because of the qualitative nature of color measurement [8].

Lehmann et al. [9] studied quantitative colorimetry during angioscopy using two color coordinates and HSI (hue, saturation, intensity) color space (see http://www.en.wikipedia.org/wiki/HSL_color_space), and utilized it to differentiate thrombus based on color [10]. However, this system was not used to distinguish atherosclerotic plaques, which have a different range of color from thrombus. Miyamoto et al. [11] found an inverse relationship between yellow color saturation and the cap thickness of fibroatheromas. In their system, yellow saturation, derived from HSI color space, was used to represent yellow color intensity of plaques (see, http://www.en.wikipedia.org/wiki/Saturation_%28 color_theory%29). However, yellow saturation may not ideally represent the gradations of yellow color intensity because of its non-linear nature. In addition, the detailed process of optimization against the effect of variables unique to angioscopy was not examined in their system.

The International Committee on Illumination (CIE) 1976 color difference formula (L*a*b* color space) has been widely used to describe all the colors visible to the human eye (see, http://www.en.wikipedia.org/wiki/Lab_color_space). In this color space, yellow color intensity and brightness can be represented simply as positive b* and L* values. Because of its linear nature, quantitative colorimetry using this color space may be a practical method to detect LCTCs during angioscopy. Therefore, we tested in an experimental model the ability of a quantitative colorimetric system based on the L*a*b* color space to measure yellow color intensity of atherosclerotic plaques during angioscopy, and used this system to characterize the color of LCTCs.

Methods

Image acquisition system

Clinically available angioscope catheters (Vecmova, Clinical Supply Co., Gifu, Japan) were used. The imaging bundle in the catheter consists of 3,000 individual silica optical fibers and the lens allows a field of view of 70° with an imaging depth >2 mm. The rest of the system includes a xenon lamplight source (Baxter OPTX 300, Baxter Laboratories, Irvine, CA) and a charge-coupled device (CCD) camera with National Television System Committee (NTSC) color system (Baxter OPTX 5000, Baxter laboratories). When white balancing, dry white paint oil (Pure White of Designers Gouache, Winsor & Newton, London, UK) was used, and light intensity was adjusted to the maximum to enhance the white color at the periphery of the image field.

Quantitative colorimetric system

The video signal was converted from analog to digital (A/D) by a converter (ADVC-100, Canopus Co., Kobe, Japan), which was directly connected to both the S (Y/C) signal output of the CCD camera and the 6 pin IEEE1394 connector of a laptop computer (Macintosh Powerbook G4, Apple Computer, Inc. CA). The display of the laptop computer was adjusted to the color temperature = CIE D65 (based on the color temperature of xenon light) and the gamma = 2.2 (based on the definition in NTSC system) for the better visualization of image color. The custom software based on the L*a*b* color space was installed into the computer, which allows the acquisition of a single frame image (a bitmap format) while preserving the red, green and blue (RGB) values from the CCD camera independently of the color setting in the computer, and permits the user to select a point of interest (POI) or a freehanded/rectangular/circular region of interest (ROI). The conversion from RGB values into L*a*b* values was programmed according to established formulae. In the L*a*b* color space, L* describes brightness of the color (–100 to 100). A positive value of a* describes redness of the color (0 to 100), a negative a* greenness (–100 to 0). Similarly, yellowness or blueness is expressed by coordinate b*, which is positive for yellow (0 to 100) and negative for blue (–100 to 0). The L*a*b* values for each pixel and the mean values with standard deviation (SD) in the selected ROI were expressed automatically.

Materials

In-vitro imaging sample

Three circular shaped standard color calibration samples with different color intensity (SCS-OR010, CY010 and VI010, Spectralon, Labsphere, North Sutton, NH) were prepared. The samples were placed on a platform and the angioscope catheter was suspended over the samples in a movable lever.

Ex-vivo yellow plaque model

Six porcine carotid arteries were isolated and dissected from Yorkshire swine. The Animal Care and Use Committee of Tufts New England Medical Center approved all procedures. In five formalin fixed carotid arteries, yellow paint oil (Primary Yellow of Designers Gouache, WINSOR & NEWTON, London, England) was dropped at a distal end of each artery to recreate yellow plaque models. The control sample was produced by dropping yellow paint oil on a flat plastic plate.

Ex-vivo human tissue sample

The specimens of seven carotid and three femoral arteries, excised during surgical endarterectomy from 10 patients (age 72–80 years, four males and six females), were used. Written informed consent to study excised tissue was obtained from all patients before the surgical procedure. The Institutional Review Board of Tufts New England Medical Center approved the protocol. The excised specimens were washed with saline, and 5–10 mm long by 3–6 mm wide samples were obtained from each specimen. The sample was placed in a platform attached with the scale, and the angioscope catheter was suspended over the sample in a rotating lever.

Experimental design

Determination of the optimal range of L*value to measure color

In this quantitative colorimetric system, the L*a*b* values are calculated from the RGB values. However, these RGB values can be affected, to some extent, by the components of the image acquisition system. Therefore, we examined if the RGB values were within the appropriate range for this calculation. In a fully darkened room, images of the standard sample SCS-OR010 were acquired perpendicularly under varying light intensity and distance from the

angioscope lens to the sample (3–15 mm at 1 mm intervals). These two variables were selected because they can directly affect brightness and can be visually manipulated during angioscopy in vivo. L* values were measured in all images at the same POI, and the relation of these two variables with L* values was examined.

Theoretically, within the L*a*b* color space, b* values can be represented independently of L* value. However, there are functional limitations of the CCD camera, in which an image with too high or low brightness can cause either a loss of the color or a non-linear portion of the video transfer function [11], suggesting that extreme values of L* can lead to inaccurate b* values. Therefore, to establish the optimal range of brightness L* for measuring the color, 100 images of each of the three standard samples were acquired perpendicularly at 10 different levels of light intensity and at 10 different distances from the scope lens to the sample in a fully darkened room. In each sample, the same POI in all 100 images was selected at two locations, and L* and b* values were measured in all images at 200 POIs. The range of L* values, at which measured b* values were constant, was determined from this relationship to be the "optimal brightness L*". Then, to evaluate the ability to differentiate color intensity after adjusting for brightness L*, the measured b* values with optimal brightness L* from each sample were compared with each other and with the actual b* value as known by spectroradiometry under the color temperature CIE D65.

Adjustment of brightness L* for angle of imaging and POI within the field of view

A prior study reported that the perception of color could be affected by the angle of the angioscope to the plaque surface [11], indicating that if the lesion is bigger and protrudes into the artery, such lesion may have increased yellow color intensity. Another study also showed the possible effect of the POI within the field of view [9] (i.e., center of the image versus edge), because of a light diffuser at the tip of the angioscope to reduce illumination to the edge in comparison to the center. Therefore, we explored whether adjusting brightness L* can overcome the variations in the perception of color.

(a) Angle

An image of the standard sample SCS-OR010 was acquired at four different angles (90°, 60°, 45°, 30°) under fixed light intensity and distance (3 mm) from the angioscope lens to the center of the circular sample. The whole field of view (about 26,000 pixels) was selected as the ROI, and the corresponding L* and b* values were obtained for the different angles. To test the effect of adjusting brightness L* on the b* value measurement under different angles, L* and b* values were measured in circular areas (each consisting of 600–700 pixels, which is based on the commonly observed area of yellow plaques in patients) at the center of the sample, at 90°, 60°, 45°, and 30° under a fixed distance (3 mm) from the angioscope lens to the center of the circular sample. Brightness L* was adjusted by varying the light intensity and judged to be adequate when the mean value of measured L* in the ROI was within the optimal range that was established in the prior study of the relationship between brightness and color. The measured values in the image at 90° were used as controls and compared with those at the other angles.

(b) POI

An image of the standard sample SCS-OR010 was acquired perpendicularly under fixed light intensity at a distance of 3 mm from the angioscope lens to the sample, and 10 equidistant points were established from the center of the image to the edge of the field of view as illustrated in Fig. 3(a). To test the effect of adjusting brightness L* on the b* value measurement at the different POI, for each of the 10 points, an image was acquired perpendicularly at a fixed distance (3 mm), and the obtained L* value at each POI was adjusted to its optimal range by varying the light intensity. The measured b* values from the 10 POI with adjusted brightness L* were analyzed for their distribution and compared with the unadjusted values.

Reproducibility of color measurement in an artificial plaque model

When analyzing color in vivo, there are also variables affecting the perception of color, such as variability between each angioscope and white balancing [9]. Therefore, to test for such variables in each "plaque", imaging was performed five times using a different angioscope with white balancing each time. The images were acquired from a proximal to distal direction in the artery and perpendicularly in the control sample. A rectangular area within the "plaque" (each consisting of 600–700 pixels) was selected as a ROI from on-line images, and light intensity and the distance from the angioscope lens to the "plaque" were adjusted manually to obtain the optimal brightness L*. Because selected ROIs could still have pixels without optimal L* values, such pixels were excluded, and the obtained b* values were analyzed for their distribution and were compared with those from the control sample.

The remaining porcine carotid artery was used to examine possible differences between images obtained in air and in injected physiologic saline solution to simulate clinical practice. The same segment of the artery was observed under each circumstance with the same angioscope and white balancing, and a circular area corresponding to 600–700 pixels was selected as a ROI. Light intensity and the distance from the angioscope lens to the surface were fixed with optimal brightness L*. After the exclusion of pixels without optimal L* values, the obtained L* and b* values were compared.

Histologic study using quantitative colorimetry

To test the ability of quantitative colorimetry to detect LCTCs, we examined the surface color in human tissue samples of atherosclerotic plaques.

(a) Procedure

The distance from the angioscope lens and the angle of the angioscope to the sample were fixed at 3 mm and 45°, respectively. Images of the sample were acquired longitudinally. The vertical center of the circular angioscopic image was aligned to the reference of the scale at 3 mm intervals from the distal 1 mm of the proximal edge of the sample. Also, at each interval, 1–3 images were obtained horizontally in order to acquire the whole width of the sample. On an acquired on-line image, a rectangular area corresponding to 800–1,200 pixels out of the whole circular angioscopic image was selected as the ROI if it had homogeneous color visually. The vertical center of both the ROI and the whole circular angioscopic image were the same. At the ROI, intensity of light was adjusted manually to obtain adequate brightness L*, which was judged to be optimal when the mean value with SD of brightness L* was within the optimal range. Then, the pixels without optimal range were excluded from the selected ROI. The ROI setting and the measurement of the color were performed two times. Intra-observer agreement for b* values was $r = 0.994$ ($P < 0.0001$). Then, the final obtained mean values of b* were expressed as the quantified color of each ROI in the blue–yellow axis.

(b) Histopathologic processing of tissue samples

After the image acquisition by angioscopy, the sample was snap-frozen in liquid nitrogen. At that time, the sample was fixed carefully on a piece of cucumber, as the transverse sections perpendicular to the long axis would be the cutting direction. Each sample was stored at –80°C, and then, was cut into 6-μm transverse sections at 3 mm longitudinal intervals, so that the crosscut images of the histopathology slices would correspond with the vertical center of the angioscopic ROI. Staining was performed with Hematoxylin-Eosin and Masson's trichrome. Eighty-eight histopathology slices corresponding to angioscopic ROIs could be collected. Based on the lesion classification by the American Heart Association [12], the single most predominant histopathologic feature for each slice was determined by the concordance of two specialists who were blinded to the angioscopic images, and categorized as follows: (1) Type 1 (initial lesion or preatheroma) = 10; (2) Type 2 (fibrous plaque or calcified plaque) = 43; (3) Type

3 (atheroma or fibroatheroma) = 30; (4) Type 4 (lesion with hemorrhage) = 5.

(c) Measurement of fibrous cap thickness

Images of histopathology slices were acquired by using the standard microscope and image software (Image-Pro Plus, version 4.1, Media Cybernetics, MD). Both angioscopy and histopathology images were composed by the image software (Adobe Photoshop 5.0) on the slide sheet (Microsoft Power Point X for Mac). Then, the location in the histopathology slice, identical with the angioscopic ROI, was identified by fitting the breadth of both angioscopy and histopathology images of the sample, and/or by the adjustment of the configuration. At the determined locations, if the lipid core underneath the fibrous cap could be identified, the fibrous cap thickness was measured at five different fibrous cap sites over the lipid core in 100× magnification images. The mean value of these five measurements was expressed as the fibrous cap thickness.

Statistical analysis

Continuous variables were presented as the mean value ±SD, or as the median value with 25th and 75th percentiles when appropriate. Correlation and group differences of continuous variables were assessed with Pearson's correlation coefficient, two-tailed *t*-test or Mann-Whitney *U*-test and *F* test for variance. A value of <0.05 was considered to indicate statistical significance.

Results

Optimal range of L*value to measure color

Brightness L* value was directly proportional to the degree of light intensity and inversely proportional to the distance from the scope to the sample [Fig. 1(a) and 1(b)], suggesting that the RGB values from the image acquisition system were appropriate for the calculation in the software program. b* value was approximately constant when L* value was within 40–80 [OR010: $b^* = 55.58 + 0.003L^*$, $r = 0.86$ ($n = 95$); CY010: $b^* = -32.88 + 0.004L^*$, $r = 0.82$ ($n = 100$); VI010: $b^* = -47.21 + 0.04L^*$, $r = 0.87$ ($n = 102$)] (Fig. 2). Within this optimal range of L*, there were significant differences in measured b* values between the three standard samples, as expected from their spectroradiometric characteristics (Table 1).

Adjustment of brightness L* for angle and POI

(a) Angle (Table 2)

With unadjusted L*, b* values at 90° and 60° were not significantly different ($P = 0.65$), however, b* values at 45° and 30° were significantly lower than that at 90° ($P < 0.0001$ for both). When L* value of the ROI was adjusted to within 40–80, there was no statistical difference in b* values between control at 90° and all other angles.

(b) POI

Brightness L* decreased from the center to the edge of the field of view, and b* values decreased towards the edge of the field of view when brightness L* was <40 [Fig. 3(b)]. However, adjusting L* value to within 40–80 (64.4 ± 7.09), resulted in a decrease in the variance of b* values [52.00 ± 9.65 before adjustment to 55.88 ± 3.48, $P = 0.03$ for the variance, Fig. 3(c)].

Reproducibility of color measurement in the yellow plaque model

For the ROI in each plaque model (Fig. 4), the mean percent of pixels excluded (L* outside 40–80), as well as the adjusted L* value, are shown on Table 3. b* values were not significantly different between the control and the five plaque models. In images in air and in saline solution, b* values were not significantly different for L* values within 40–80 (Table 3).

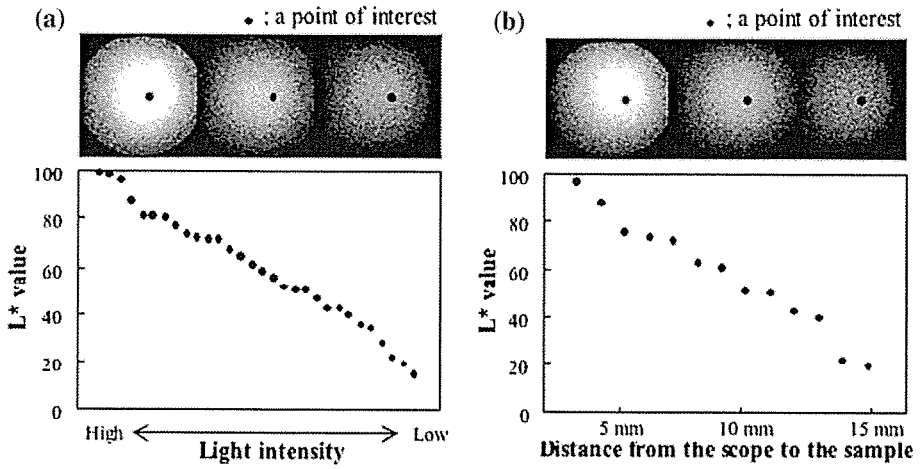

Fig. 1 Brightness L* value in relation to intensity of light (**a**) and distance from the angioscope to the sample (**b**). L* value was directly proportional to the degree of light intensity and inversely proportional to the distance from the scope to the sample

High yellow color intensity and LCTCs

Disruption or thrombus was not detected by histology in any of the samples (Fig. 5).

The median value of b* in each histopathology type was as follows: Type 1: –17.67 (–18.34 to –8.17); Type 2: –13.10 (–11.70 to –4.89); Type 3: 17.90 (10.44 to 18.83); Type 4: –24.39 (–25.16 to –22.06) (Fig. 6). The b* value of Type 3 was significantly higher than those of the other types ($P = 0.0002$ vs. Type 1; $P < 0.0001$ vs. Type 2 and Type 4, respectively). Among 43 Type 2 samples, nine calcified plaques had a clearly defined lipid core underneath a fibrous cap, and the b* value of these nine plaques [20.45 (14.35–26.29)] was not significantly different as compared with that of Type 3 ($P = 0.42$).

In the 38 samples with an identified lipid core underneath a fibrous cap (9 of 43 Type 2 and 29 of 30 Type 3), not including the Type 4 lesions (Fig. 7), b* value demonstrated an inverse linear correlation with the fibrous cap thickness (b* = 27.60–0.61 × fibrous cap thickness, $r = 0.51$, $P = 0.001$). In the 13 samples with a fibrous cap thickness <100 μm (10 fibroatheromas and three calcified plaques), the b* values were all ≥23 (35.91 ± 8.13).

In all Type 4 lesions, hemorrhage was detected in a lipid core by histopathology, and a visually dark blue appearance was seen in the ROIs of angioscopy (Fig. 5). The thickness of the fibrous cap was <100 μm (84.82 μm) in one of five samples, and >100 μm (175.22 ± 51.09 μm) in the remaining samples.

Discussion

We describe a quantitative colorimetric system based on the L*a*b* color space that could consistently measure atherosclerotic plaque color after proper adjustments for brightness. These adjustments are necessary because of changes in color perception that occur due to a number of variables unique to angioscopy, such as changes in light intensity, distance, and even the angle of the angioscope to the ROI. Our results revealed that the impact of these variables on color perception could be minimized by the brightness L* adjustment. In human atherosclerotic plaques, we found that high b* value (high yellow color intensity), determined by this quantitative colorimetric system, was associated with LCTCs.

Yellow plaque is thought to possess features commonly attributed to the atherosclerotic plaques vulnerable to thrombosis. Yellow color correlates with lipid-rich atheromas and thin fibrous caps [3, 4, 11]. Yellow coronary lesions have increased distensibility and are associated with compensatory outward remodeling [13],

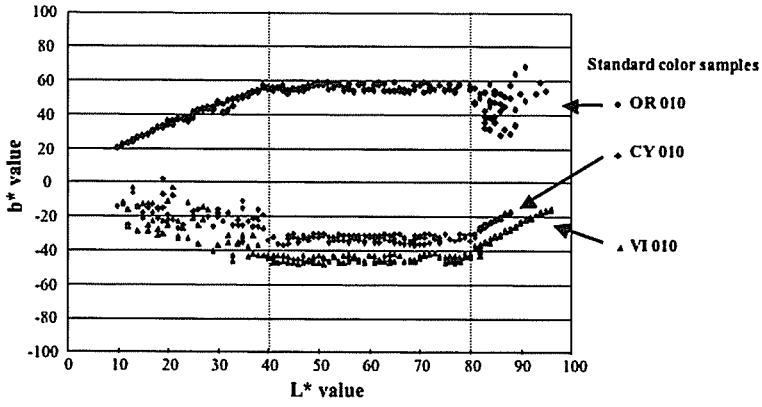

Fig. 2 In each of the three standard samples, b* value (yellow color intensity) was constant when L* was within 40–80

Table 1 Comparison of measured L*, b* values of standard color samples with quantitative colorimetry and actual values

Samples	Adjusted L* value	Measured b* value	Actual b* value
SCS-OR010	58.86 ± 11.70	55.73 ± 1.67**	43.74
SCS-CY010	61.21 ± 10.44	-32.63 ± 1.97**	-11.06
SCS-VI010	60.21 ± 12.32	-44.78 ± 1.69**	-22.77

Actual values are from spectroradiometry. **$P < 0.0001$; SCS-OR010 vs. CY010 or VI010; SCS-CY010 vs. VI010

Table 2 Comparison of b* values with non-adjusted or adjusted L* at various angles

Degree	L* value	b* value	*P* value for b* value vs. 90°
Non-adjusted			
90°	41.80 ± 20.92	34.64 ± 20.24	–
60°	30.64 ± 21.17	32.23 ± 19.30	0.65
45°	26.94 ± 20.60	28.96 ± 19.83	<0.0001
30°	22.28 ± 20.72	22.83 ± 19.05	<0.0001
Adjusted			
90°	68.89 ± 6.30	59.74 ± 8.56	–
60°	66.82 ± 6.01	60.56 ± 7.66	0.12
45°	63.54 ± 6.46	58.45 ± 8.11	0.11
30°	60.69 ± 6.90	57.18 ± 8.61	0.09

which may confer mechanical and structural weakness to the plaque. The plaque underlying coronary thrombus is usually yellow and/or disrupted as assessed by angioscopy [7], and these plaques are associated with higher frequency of adverse events after percutaneous coronary intervention [6], perhaps due to their thrombogenic nature. Multiple yellow plaques have been observed by angioscopy in non-culprit sites in patients with myocardial infarction [14], in support of the concept of pan-coronary vulnerability. Moreover, a clinical study demonstrated an association of yellow plaque with a higher incidence of future acute myocardial infarction [4], in which "glistening" yellow plaques were more likely to become future culprit lesions. Our previous study suggested that plaque color changes from yellow to white might indicate plaque stabilization by lipid-lowering therapy [15]. Thus, the body of evidence suggests that yellow color may be indicative of vulnerable coronary lesions. However, plaque color assessment has traditionally been made subjectively, which has become one of the Achilles' heels of angioscopy to study a possible association between yellow lesion and vulnerability. Our findings indicate that the quantitative colorimetric system based on the L*a*b* color space could be used to consistently measure the color of atherosclerotic plaques during angioscopy.

In the experimental conditions, measured color of the standard calibration samples differed from the actual values by spectroradiometry because of the following possible sources of error of the color signal: (1) the optic fibers; (2) the xenon lamplight; (3) the CCD camera; (4) white balancing without the equal energy white color standard (which is difficult to preserve and is expensive, thus not convenient for clinical use); and (5) the theoretical correction processes for the light

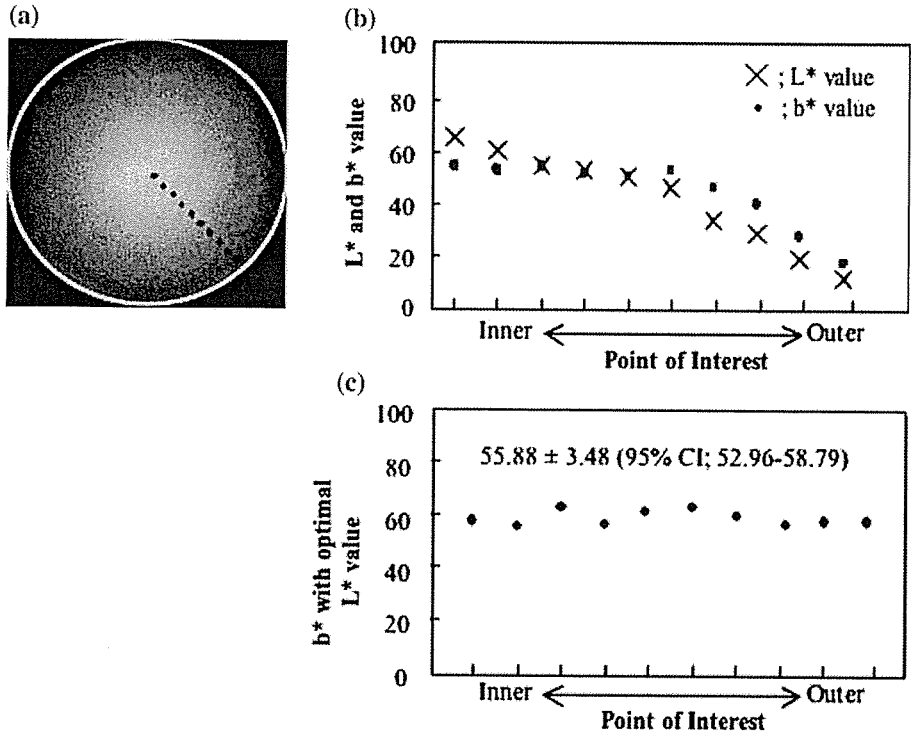

Fig. 3 (**a**) Displays 10 points of interest (POI) within the field of view from center to edge. (**b**) Unadjusted L* and b* values decreased from the center of the field of view to the edge. (**c**) After adjusting for L*, b* was similar among the different POI

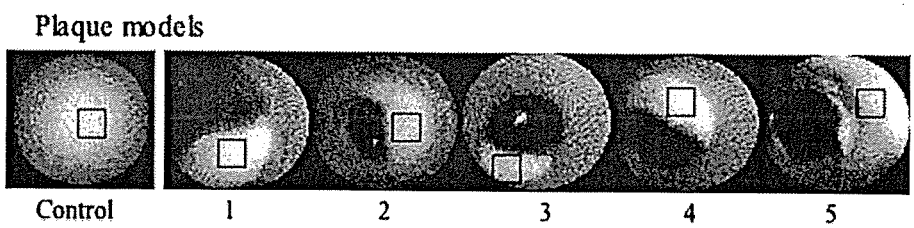

Fig. 4 Artificial yellow plaque models in porcine carotid arteries. A rectangular circle shows a region of interest

Table 3 Comparison of b* values with adjusted L* between various plaque models or between in air and in saline solution

	% Pixels excluded in ROI (L* outside 40–80)	Adjusted L* value	b* value	*P* value for b* value
Plaque models				*Versus Control*
Control	8.8	66.74 ± 8.02	67.54 ± 3.25	–
1	9.1	64.51 ± 8.54	66.07 ± 3.92	0.12
2	8.6	66.60 ± 8.35	67.76 ± 3.83	0.93
3	6.5	64.67 ± 8.30	66.04 ± 3.76	0.10
4	8.9	64.88 ± 9.39	66.18 ± 4.64	0.55
5	8.6	64.50 ± 10.23	65.18 ± 5.04	0.08
Air/Saline				*Versus air*
Air	6.8	58.50 ± 12.54	–7.27 ± 2.85	–
Saline solution	7.5	58.13 ± 11.32	–7.40 ± 2.68	0.66

ROI = region of interest

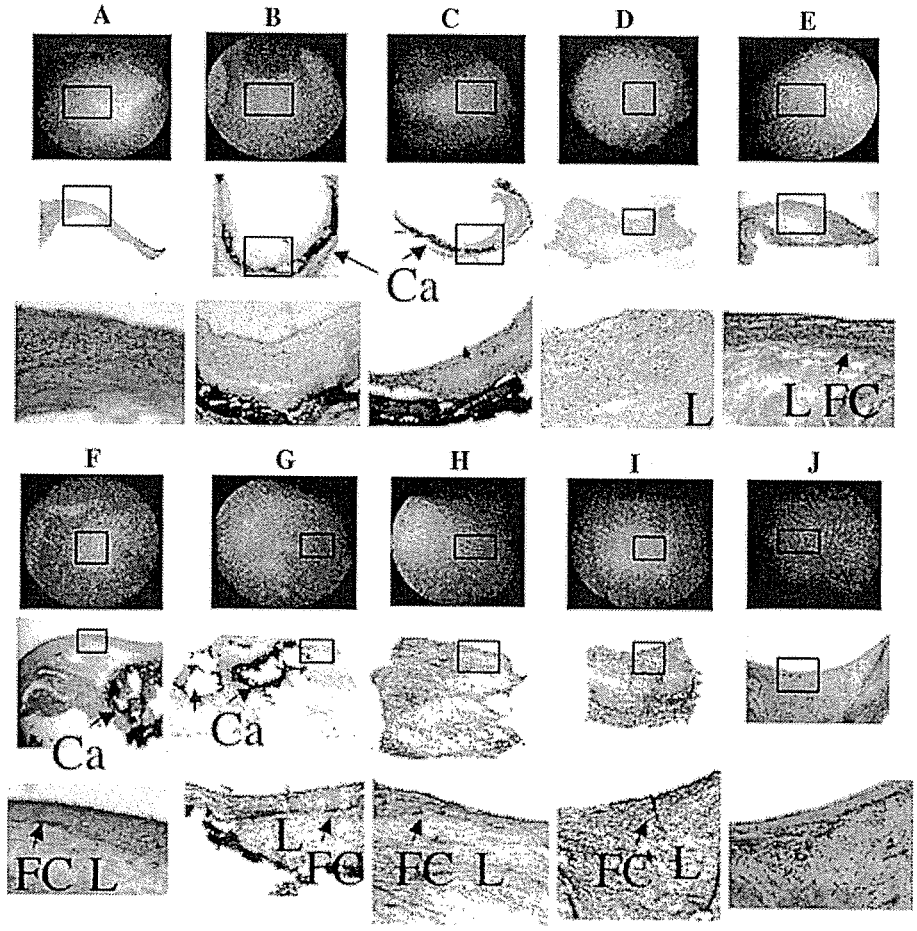

Fig. 5 Upper pictures show angioscopy images and the rectangular circles indicate the regions of interest (ROI). Middle pictures (H&E or Masson's trichrome stain, 12.5×) show the corresponding histology slices and the rectangular circles indicate the locations corresponding to the ROI of angioscopy images. Lower pictures (H&E or Masson's trichrome stain, 100×) show the larger view of the rectangular circles in the middle pictures. Ca = calcium, L = lipid core, FC = fibrous cap. (**A**) intimal lesion; (**B**) fibrous lesion; (**C**), (**F**), (**G**) calcified lesion; (**D**) atheroma; (**E**), (**H**), (**I**) fibroatheroma; (**J**) lesion with hemorrhage

temperature or the gamma value. It is complicated to quantify color completely using current angioscopic systems because of the multidimensional characteristics of color. However, in our study, we used the A/D converter and the computer software without the original color correction circuit. All images during white balancing were analyzed and L*, a* and b* values were 100, 0 and 0 in the whole field of view (data not shown), suggesting that each white balancing process was the same. By using L*a*b* color space, L* values were useful, as brightness was used to determine the optimal condition during the procedures of not only image acquisition but also of image analysis. In addition, the different color intensity of standard color samples could be measured through the same algorithm with minimum variances. Therefore, this system can be acceptable for consistent measurement of color during angioscopy, which is consistent with the study by Lehmann et al. [9, 10], and the quantified value can be compared between different atherosclerotic plaques.

Our findings indicate that high yellow color intensity, determined by b* values, could be used as a surrogate for the structural change of LCTCs in atherosclerotic plaques. The association of yellow color with a lipid core is consistent with prior

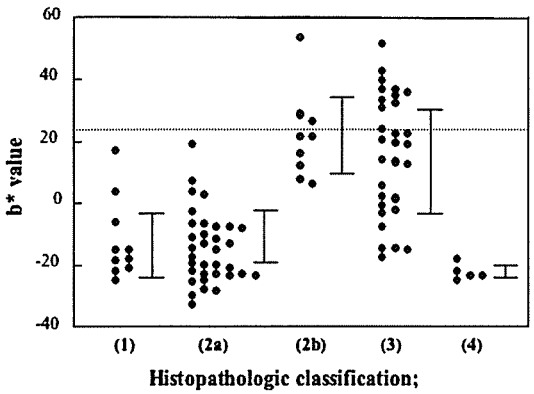

(1) Type 1=initial lesion, fatty streak and preatheroma (n=10).
(2a) Type 2 without lipid cores underneath fibrous caps (n=34).
(2b) Type 2 with lipid cores underneath fibrous caps (n=9).
(Type 2=fibrous and calcified plaque).
(3) Type 3=atheroma and fibroatheroma (n=30).
(4) Type 4=lesion with hemorrhage (n=5).

Fig. 6 b* value was higher in Type 3 (atheroma/fibroatheroma) lesions. Among 43 Type 2 (fibrous/calcified plaque) lesions, nine calcified plaques had lipid cores underneath fibrous caps, and yellow color intensity of these nine plaques was comparable with Type 3 [$P < 0.0001$ for (3) vs. (1) and (2), (2) vs. (4); $P = 0.0002$ for (1) vs. (4); $P < 0.0001$for (5) vs. (3) and (4)]

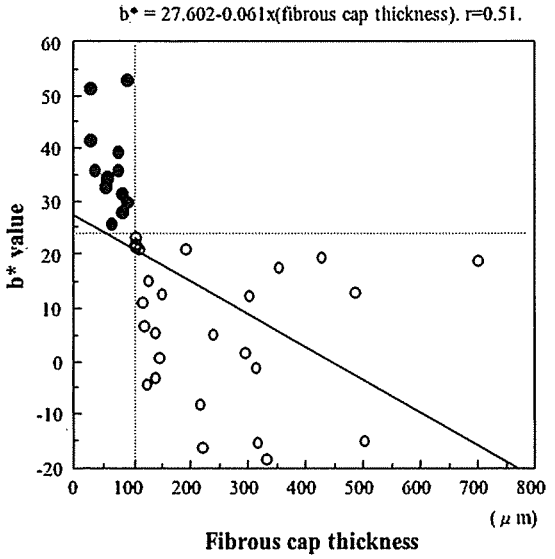

Tissue samples with identifiable lipid cores underneath thin fibrous caps (n = 38)

Fig. 7 Among 38 regions [9 Type 2 (fibrous/calcified plaque) and 29 Type 3 (atheroma/fibroatheroma) with identified lipid cores underneath fibrous caps], b* value demonstrated an inverse linear correlation with the fibrous cap thickness covering the lipid core. Yellow color intensity was high (b* ≥ 23: represented by black circles) in all locations with the fibrous cap thickness < 100 μm

angioscopy studies [3, 4]. However, the dispersion of yellow color among various types of plaque in our study suggests that surface yellow color may be determined not only by a lipid core but also by the various degrees of superficial intra- or extra-cellular lipids, consistent with histopathologic studies [12], because intimal cholesterol in human atherosclerotic plaques, in general, contains β-carotene that are yellow colored lipids [16]. The strong association between high yellow color intensity and LCTCs in our study is in line with the study by Miyamoto et al. [11], in which the percent saturation of yellow color increased inversely with the thickness of fibrous caps in fibroatheromas. Our results indicate that, once the fibrous cap above a lipid core becomes thinner than 100 μm, both the lipid core and the thin fibrous cap determine high yellow color intensity at such region. Our study also suggests that high yellow color intensity regions may be independent of the deeper segmental histopathology. Miyamoto et al. suggested that yellow color of the plaque surface reflects the presence of lipid pools up to 300 (m in depth [11]. Kawasaki et al. also demonstrated that visually assessed deep yellow color of coronary plaques was associated only with a thin fibrous cap above a lipid core, using both angioscopy and integrated backscatter analysis by intravascular ultrasound [17]. Thus, high yellow color intensity regions may not necessarily represent thin-cap fibroatheromas, the most common type of suspected vulnerable plaques based on histologic studies [18], but LCTC in a certain area of atherosclerotic plaques. This gives further support to the association of yellow plaque color with thrombus seen in clinical studies [3–8], because lipid cores are thrombogenic [19]. An exception would be lesions with severe intraplaque hemorrhage near the surface area, as LCTCs in these lesions did not appear yellow but bluish, perhaps because the surface color of tissue samples could change from red to violet by the deoxygenated blood component [20]. These lesions may have a reddish discoloration in vivo, as suggested by the study of Thieme et al. [3], in which a yellow–red plaque color was associated with atheroma or degenerated plaques with patchy necrosis. It is thus possible that red color appearance of plaque may also be useful to identify high-risk coronary sites.

A recent study indicated the possible link between intraplaque hemorrhage and plaque vulnerability prone to thrombosis [21], and yet another study suggested that angioscopy can be used to detect macrophage infiltration [22].

There are several limitations in the present study. First, we used three standard color samples with rather different b* values, which may limit the interpretation of the ability of our system to provide a precise discrimination between colors. However, the association between high yellow color intensity and LCTCs suggests that it may be acceptable for characterization of LCTCs as discussed above. Second, although the image acquisition of tissue samples was performed shortly after excision, changes in b* value must be considered because, if the blood component was rich near the surface area, the surface color may be expressed as a lower b* value (bluish hue) in tissue samples [20]. However, the fact that high b* values were measured in LCTCs suggests that this effect may not have a significant impact on the association of high b* value with LCTCs. Third, the materials of endarterectomy specimens in human atherosclerotic plaques of carotid or femoral arteries may limit the application of the association of high yellow color intensity with LCTCs to coronary arteries, and the number of specimens were relatively small, Further validation of high yellow color intensity regions will be required in ex-vivo and in-vivo human coronary arteries.

In the clinical setting, quantitative colorimetry during angioscopy could be useful to evaluate the possible relationship of LCTCs with plaque vulnerability by investigating their natural history. The clinical utility of angioscopy is limited to selected patients, since angioscopy as a routine imaging technique is impractical because of its invasive nature and the potential risk during the examination as displacement of blood is required [23]. Nevertheless, it can be useful as a research tool for vulnerable plaque and may guide novel diagnostic and therapeutic modalities in high-risk patients.

Conclusions

Atherosclerotic plaque color can be consistently measured with this quantitative colorimetric system based on the L*a*b* color space during angioscopy, if adjustments are made for brightness. High yellow color intensity, determined by this system, was associated with LCTCs. Therefore, angioscopy with quantitative colorimetry may be useful to detect LCTCs, which may be markers of vulnerable plaques.

Acknowledgements This study was supported in part by Research Grants from Fukuda Kinenn Foundation (to F.I) and for Cardiovascular Disease (15-5) from The Japanese Ministry of Health, Labor and Welfare (to K.M).

References

1. Falk E (2006) Pathogenesis of atherosclerosis. J Am Coll Cardiol 47:C7–C12
2. Waxman S, Ishibashi F, Muller JE (2006) Detection and treatment of vulnerable plaques and vulnerable patients: novel approaches to prevention of coronary events. Circulation 114:2390–2411
3. Thieme T, Wernecke KD, Meyer R et al (1996) Angioscopic evaluation of atherosclerotic plaques: validation by histomorphologic analysis and association with stable and unstable coronary syndromes. J Am Coll Cardiol 28:1–6
4. Uchida Y, Nakamura F, Tomaru T et al (1995) Prediction of acute coronary syndromes by percutaneous coronary angioscopy in patients with stable angina. Am Heart J 130:195–203
5. Mizuno K, Miyamoto A, Satomura K et al (1991) Angioscopic coronary macromorphology in patients with acute coronary disorders. Lancet 337:809–812
6. Waxman S, Sassower M, Mittleman M et al (1996) Angioscopic predictors of early adverse outcome following coronary angioplasty in patients with unstable angina and non-Q wave myocardial infarction. Circulation 93:2106–2113
7. Waxman S, Mittleman MA, Zarich SW et al (1997) Angioscopic assessment of coronary lesions underlying thrombus. Am J Cardiol 79:1106–1109
8. den Heijer PJ, Foley DP, Hillege HL et al (1994) The "Ermenonville" classification of observations at coronary angioscopy: evaluation of intra-and inter-observer agreement. European Working Group on Coronary Angioscopy. Eur Heart J 15:815–818
9. Lehmann KG, Oomen JA, Slager CJ et al (1998) Chromatic distortion during angioscopy: assessment and correction by quantitative colorimetric angioscopic analysis. Cathet Cardiovasc Diagn 45:191–201
10. Lehmann KG, van Suylen RJ, Stibbe J et al (1997) Composition of human thrombus assessed by quantitative colorimetric angioscopic analysis. Circulation 96:3030–3041
11. Miyamoto A, Prieto AR, Friedl SE et al (2004) Atheromatous plaque cap thickness can be determined by quantitative color analysis during

angioscopy: implications for identifying the vulnerable plaque. Clin Cardiol 27:9–15
12. Stary HC, Chandler AB, Dinsmore RE et al (1995) A definition of advanced types of atherosclerotic lesions and a histological classification of atherosclerosis. A report from the Committee on Vascular Lesions of the Council on Arteriosclerosis, American Heart Association. Circulation 92:1355–1374
13. Takano M, Mizuno K, Okamatsu K et al (2001) Mechanical and structural characteristics of vulnerable plaques: analysis by coronary angioscopy and intravascular ultrasound. J Am Coll Cardiol 38:99–104
14. Asakura M, Ueda Y, Yamaguchi O et al (2001) Extensive development of vulnerable plaques as a pan-coronary process in patients with myocardial infarction: an angioscopic study. J Am Coll Cardiol 37:1284–1288
15. Takano M, Mizuno K, Yokoyama S et al (2003) Changes in coronary plaque color and morphology by lipid-lowering therapy with atorvastatin: serial evaluation by coronary angioscopy. J Am Coll Cardiol 42:680–686
16. Blankenhorn DH, Freiman DG, Knowle HC (1956) Cartenoids in man: the distribution of epiphasic cartenoids in atherosclerotic lesions. J Clin Invest 35:1243–1247
17. Kawasaki M, Takatsu H, Noda T et al (2002) In vivo quantitative tissue characterization of human coronary arterial plaques by use of integrated backscatter intravascular ultrasound and comparison with angioscopic findings. Circulation 105:2487–2492
18. Virmani R, Kolodgie FD, Burke AP et al (2000) Lessons from sudden coronary death: a comprehensive morphological classification scheme for atherosclerotic lesions. Arterioscler Thromb Vasc Biol 20:1262–1275
19. Fernandez-Ortiz A, Badimon JJ, Falk E et al (1994) Characterization of the relative thrombogenicity of atherosclerotic plaque components: implications for consequences of plaque rupture. J Am Coll Cardiol 23:1562–1569
20. Kienle A, Lilge L, Vitkin IA et al (1996) Why do veins appear blue? A new look as an old question. Appl Optics 35:1151–1160
21. Kockx MK, Cromheeke KM, Knaapen MWM et al (2003) Phagocytosis and macrophage activation associated with hemorrhagic microvessels in human atherosclerosis. Arterioscler Thromb Vasc Biol 23:440–446
22. Kurita A, Ishizuka T, Matsui T et al (2004) Significance of angioscopic morphology for the estimation of macrophage infiltration and vascular physiology. Int J Cardiovasc Imag 20:165–171
23. Ishibashi F, Aziz K, Abela GS et al (2006) Update on coronary angioscopy: review of a 20-year experience and potential application for detection of vulnerable plaque. J Intervent Cardiol 19:17–25

European Heart Journal (2006) 27, 2189–2195
doi:10.1093/eurheartj/ehl181

Angioscopic differences in neointimal coverage and in persistence of thrombus between sirolimus-eluting stents and bare metal stents after a 6-month implantation

Masamichi Takano, Takayoshi Ohba, Shigenobu Inami, Koji Seimiya, Shunta Sakai, and Kyoichi Mizuno*

Department of Internal Medicine, Chiba-Hokusoh Hospital, Nippon Medical School 1715 Kamakari, Imba, Chiba 270-1694, Japan

Received 18 February 2006; revised 15 June 2006; accepted 14 July 2006; online publish-ahead-of-print 7 August 2006

See page 2147 for the editorial comment on this article (doi:10.1093/eurheartj/ehl170)

KEYWORDS
Stent;
Neointimal hyperplasia;
Thrombus

Aims The neointimal coverage and intracoronary thrombi within stented segments at 6 months after implantation between sirolimus-eluting stents (SESs) and bare metal stents (BMSs) were compared by direct visualization using angioscopy.

Methods and results Forty-six patients (36 stable angina and 10 acute coronary syndrome) were treated with 33 SESs and 33 BMSs. Immediately after and 6 months after stenting, each of the stented segments, edge body, and overlapping segment were observed by angioscopy and the grade of neointimal coverage over the stents was classified as 0: absent neointima, 1: visible struts through thin neointima, or 2: invisible struts. The existence of thrombi was also evaluated. The average grade of the neointimal coverage at 6 months follow-up was lower in the SES than that in the BMS (edge: 1.4 ± 0.7 vs. 1.9 ± 0.2, body: 1.0 ± 0.5 vs. 1.8 ± 0.5, overlapping segment: 0.6 ± 0.7 vs. 1.8 ± 0.5; $P < 0.0001$, $P < 0.0001$, $P = 0.0069$, respectively). The frequency of persistence of thrombus was significantly higher in the SESs than that in the BMSs (86 vs. 29%, respectively; $P = 0.031$).

Conclusion The present study suggested a delayed neointimal stent coverage and slower thrombus disappearance process in the SESs in comparison to the BMSs.

Introduction

To date, stent implantation has become the standard therapy in percutaneous coronary intervention (PCI) for patients with atherosclerotic coronary disease. Nevertheless, in-stent restenosis (ISR) within 3–8 months is a factor that limits the long-term success of stenting and it is mainly caused by neointimal hyperplasia.[1] Recently, sirolimus, a cytostatic macrocyclic lactone with both anti-inflammatory and antiproliferative properties, delivered from a polymer-encapsulated stent was shown in several angiographic and intravascular ultrasound (IVUS) studies to reduce the risk of ISR in comparison with the bare metal stent (BMS).[2–8] Neointimal proliferation inside the sirolimus-eluting stent (SES), which is recognized as lumen late loss on angiograms or as an obstruction volume on the IVUS, was minimal and nearly abolished at the 6-month follow-up.[4–7] Moreover, the in-stent lumen dimensions remained essentially unchanged for a long-term without a 'late catch-up'.[9] In contrast, there have been recent concerns regarding their potential for developing late-stent thrombosis related to the delayed re-endothelialization over the struts of the SES, particularly after discontinuation of dual antiplatelet therapy.[10,11] Therefore, it is important to know when complete re-endothelialization of drug-eluting stent occurs. If complete neointimal coverage of the drug-eluting stent is accomplished, thienopyridine may no longer be needed.

Coronary angioscopy provides a direct visualization of the luminal surface and detailed information on the state of stent coverage by the neointima, changes in the plaque colour, and the existence of intracoronary thrombi.[11–15] In this study, the condition of neointimal coverage and intracoronary thrombi over SESs are compared with those observed in BMSs at 6 months after their implantation.

Methods

Patients population

Between October 2004 and April 2005, 53 patients with *de novo* and native coronary artery lesions were treated with SESs (Cypher, Cordis Corp., Miami Lakes, FL, USA). During this study period,

* Corresponding author. Tel: +81 476 99 1111; fax: +81 476 99 1863.
E-mail address: mizunok@nms.ac.jp